V European Conference on Computational Fluid Dynamics
ECCOMAS CFD 2010
J. C. F. Pereira and A. Sequeira (Eds)
Lisbon, Portugal, 14–17 June 2010

COMPARISON AND EVALUATION OF CELL-CENTERED AND CELL-VERTEX DISCRETIZATION IN THE UNSTRUCTURED TAU-CODE FOR TURBULENT VISCOUS FLOWS

Gang Wang [*], Axel Schwöppe [†], and Ralf Heinrich [††]

[*] DLR, Institute of Aerodynamics and Flow Technology,
Lilienthalplatz 7, 38108 Braunschweig, Germany.
e-mail: gang.wang@dlr.de

[†] DLR, Institute of Aerodynamics and Flow Technology,
Lilienthalplatz 7, 38108 Braunschweig, Germany.
e-mail: axel.schwoeppe@dlr.de

[††] DLR, Institute of Aerodynamics and Flow Technology,
Lilienthalplatz 7, 38108 Braunschweig, Germany.
e-mail: Ralf.heinrich@dlr.de

Key words: Unstructured Mesh, Turbulence Model, Cell-Centered Discretization, Cell-Vertex Discretization

Abstract. *The objective of this paper is to make a comparison and evaluation on cell-centered and cell-vertex discretization in the DLR TAU-code for turbulent flows. In the following, TAU with cell-vertex and cell-centered centered discretization will be called TAU-CV and TAU-CC, respectively. Starting with the analysis of differences between cell-centered and cell-vertex discretization, the merits and drawbacks of these two approaches are summarized, and then serious of typical benchmark cases covering different grid types and turbulent models are selected for the computation of TAU-CC and TAU-CV. In these test cases, the accuracy and efficiency of above two versions of TAU code are compared. Some cases show that TAU-CC and TAU-CV reveal different behaviors in prediction the location of shock wave and flow separation pattern; however, TAU-CC demonstrates comparable accuracy and efficiency as compared with TAU-CV. It is observed that the accuracy and rate of convergence of the above solvers are strongly influenced by the quality of the mesh, and it will be shown that the TAU-CC has improved convergence behavior compared with TAU-CV on meshes with sharp boundary corners. The general conclusion is that TAU-CC has strong capability for the simulation of turbulent flows and this additional option provides the TAU code with extended powerful functionalities for the simulation of complex flow problems.*

1 INTRODUCTION

In computational fluid dynamics, both cell-centered and cell-vertex discretization are successfully used in finite volume codes. Although the merits and drawbacks of these two types of discretization methods have been intensively studied in the past several decades [1-4], it is still very difficult or impossible to draw a universal conclusion that which one is a better choice for a finite volume unstructured CFD code. Actually the performance on CPU running time of above two discretization approaches highly depend on the computational environments, such as programming languages, data structures, operating systems, and so on. Thus, it is necessary and important to assess cell-centered and cell-vertex discretizations for industry flows in identical working environments. Mavriplis [1] suggest that 'a solver which can be operated in either mode' should be used in order to 'provide a more solid basis for comparing cell versus vertex-type discretizations'.

This leads to the main work of this paper: performances of cell-centered and cell-vertex discretization for simulating turbulent viscous flows were compared and evaluated by using the DLR TAU-code [5, 6]. The TAU-Code is developed for aerodynamic applications in the field of aircraft and widely use at DLR, universities and industries. In this code, the governing equations are discretized with finite volume method on unstructured hybrid meshes. The default discretization technique of the TAU-Code is based on a cell-vertex grid metric and edge-based data structures, in the following called TAU-CV. In recent years a new option of the TAU-Code using the cell-centered metric has been developed as an alternative, in the following called TAU-CC. Since TAU-CC and TAU-CV are run in exactly the same working environments, it makes the comparison and evaluation credible on the algorithm aspects, i.e., different grid types, different boundary treatments, different flux calculation schemes and different turbulence models.

In the first section of this paper, the main differences between cell-centered and cell-vertex in spatial discretization of the Reynolds averaged Navier-Stokes equations are summarized. Next a series of typical test cases covering different grid types and different turbulence models is selected for the computation with TAU-CC and TAU-CV. These test cases include the turbulent flat plate with structured mesh, the multi-element-airfoil TC11 with a hybrid unstructured mesh, the LANN wing with two different structured meshes, the DPW3-W1[7] wing with a set of hybrid mesh for grid convergence study and the DLR-F6 wing-body-fairing configuration with a hybrid mesh. The range of turbulence models used in above tests cases covers one-equation model (Spallart-Allmaras [8] type), two-equation turbulence model (k-ω type) and differential Reynolds stress turbulence model. In each test case, the accuracy and efficiency of the above two options of the TAU code are compared. Finally, several concluding remarks obtained from above evaluation works are presented.

2 NUMERICAL CONSIDERATIONS

2.1 General analysis

The basic difference between cell-centered and cell-vertex lies in the construction of control volumes. In the cell-centered grid metric, the control volumes are identical with primary grid cells, as shown in Figure 1(a), for two dimensional cases. And hence, the unknowns are defined at the cell centroids. While in the cell-vertex grid metric, the solution variables are located at the primal grid vertices, and the control volumes are reformed around each primal grid node by a median dual mesh construction, which connect the centroids of primal cells with surrounding midpoints of faces and edges, as

shown in Figure 1(b). In the TAU-Code, because the TAU-CC and TAU-CV share the same edge based data structure to store the connectivity of control volumes, this leads to the differences between them only origin from the construction features of cell-centered and cell-vertex grid metrics.

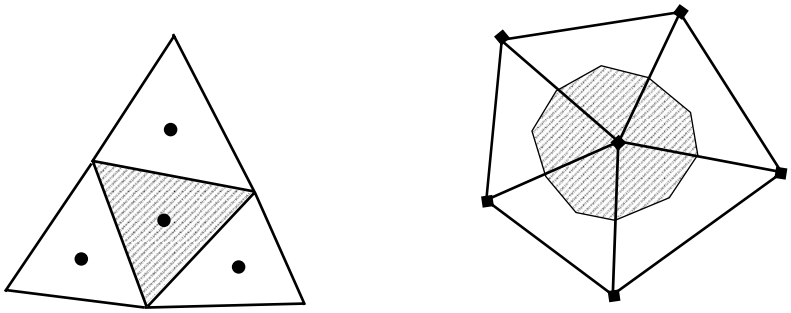

(a) (b)

Figure 1: Illustration of cell-centered (a) and cell-vertex (b) type control volume constructions.

Another principle difference between the cell-centered and cell-vertex grid metrics relates to the number of control volumes (the degrees of freedom), which is determined by the numbers of primary grid cells and vertices, respectively. It is worth noting that the ratio between numbers of primary grid cells and vertices varies with grid topology. In pure structured meshes this ratio closes to one; in pure 3D tetrahedral meshes it is in the range of 5 to 6; in typical 3D hybrid meshes, this ratio is roughly 3. This leads to the argument that the cell-centered scheme should be more accurate than the cell-vertex one on the same unstructured grid. However, a control volume in cell-centered grid metric has smaller number of neighbor cells compare to a control volume in the cell-vertex grid metric.

It has to be point out here that the construction of median dual mesh may produce control volumes with bad quality, especially for some grids with large distortions. For example, if an O-type mesh is generated at the sharp boundary corner (e.g. trailing edge of an airfoil, see Figure 2), then a series of arrow-shaped control volumes will be formed with the median dual mesh construction, which can strongly decrease the performances of the flow solvers.

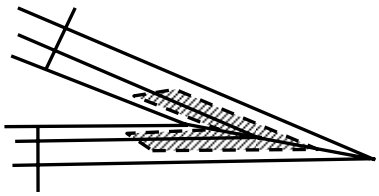

Figure 2: Illustration of dual mesh construction at sharp edge corner

In the following subsection, modifications from TAU-CV to TAU-CC on aspects of solution reconstruction, gradient evaluation and boundaries treatments will be presented in details.

2.2 Flux integration

One obvious characteristic of the cell-vertex grid metric is that the edges of the dual mesh always cross the midpoints of the face connected with two corresponding vertices, as shown in Figure 3, while in the cell-centered grid metric this property can not be

achieved in general. This advantage of the cell-vertex grid metric brings a lot of benefits in surface flux computing, especially for central discretization.

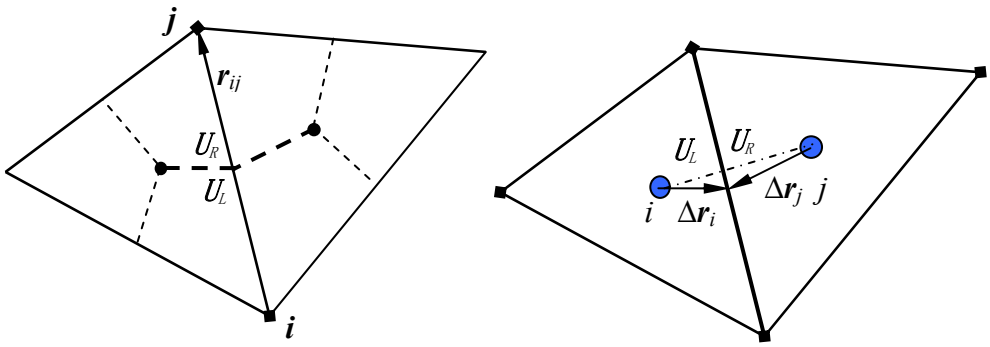

(a) Cell-vertex (b) Cell-centered

Figure 3: Solution reconstruction for TAU-CV and TAU-CC in 2D unstructured mesh

In other words, the upwind discretization seems to be a better choice for TAU-CC. For example, with the flux difference splitting scheme of Roe, the convective flux over the control volume face associate with edge *ij,* see Figure 3, can be written as:

$$\boldsymbol{F}_{ij} = \boldsymbol{F}(U_L, U_R) = \frac{1}{2}\left[\boldsymbol{F}(U_L) + \boldsymbol{F}(U_R) - \left|A_{Roe}\right|(U_R - U_L)\right]$$

To achieve second order accuracy, solution reconstruction should be used to specify the flow states on the left and the right side of each control volume surface. Several reconstruction methods have been implemented in the TAU-Code, the most commonly used method is the piecewise linear reconstruction, presented by Barth and Jespersen [9]. In this approach, the solution is assumed to have a piecewise linear distribution over the control volume, then the left and right states for TAU-CV can be reconstructed as

$$U_L = U_i + \frac{1}{2}\phi_i(\boldsymbol{r}_{ij} \cdot \nabla U_i)$$

$$U_R = U_j - \frac{1}{2}\phi_j(\boldsymbol{r}_{ij} \cdot \nabla U_j)$$

where ∇U_i is the gradient of U and ϕ_i is the value of limiter function at vertex i, $\mathbf{r}_{ij}$ represents the vector from vertex i to vertex j, as shown in Figure 3(a). The factor ½ results from the midpoint property of median dual mesh.

For TAU-CC, this approach should be modified as

$$U_L = U_i + \phi_i \Delta \boldsymbol{r}_i \cdot \nabla U_i$$

$$U_R = U_j + \phi_j \Delta \mathbf{r}_j \cdot \nabla U_j$$

here, $\Delta \boldsymbol{r}_i$ and $\Delta \mathbf{r}_j$ represent vectors pointing from cell centers to the barycentre of the control volume face, see Figure 3(b). In above procedure, TAU-CC always uses the flux at face barycentre to represent the average value over this face. In the case where the flux is a linear distribution, then the numerical flux integration is exact; however, TAU-CV has no such property because the barycentre is not defined on cell-vertex type control volume faces. Hence the above approach leads to more accurate flux integration compared to TAU-CV. Unfortunately, in boundary layer and shock wave area, this

advantage of TAU-CC is undermined because the flux in these regions usually has typical nonlinear distribution.

In viscous flux computation, both the flow variables and their gradients are required at the face associate with neighboring control volume *i* and *j*. Since gradients have been computed inside each control volume in the reconstruction process of second order upwind scheme, the gradients at the control volume face can be estimated by the following hybrid interpolation approach

$$\nabla U_{ij} = \overline{\nabla U_{ij}} - \left[\overline{\nabla U_{ij}} \cdot \boldsymbol{r}_{ij} - (U_j - U_i)\right] \frac{\boldsymbol{r}_{ij}}{\left|\boldsymbol{r}_{ij}\right|^2}$$

where $\overline{\nabla U_{ij}} = \frac{1}{2}(\nabla U_i + \nabla U_j)$ for TAU-CV. In TAU-CC, this term is slightly changed by using linear interpolation according to the distances from cell-centroids to face barycenter.

$$\overline{\nabla U_{ij}} = \frac{\left|\Delta \boldsymbol{r}_j\right|}{\left|\Delta \boldsymbol{r}_i\right| + \left|\Delta \boldsymbol{r}_j\right|} \nabla U_i + \frac{\left|\Delta \boldsymbol{r}_i\right|}{\left|\Delta \boldsymbol{r}_i\right| + \left|\Delta \boldsymbol{r}_j\right|} \nabla U_j$$

2.3 Gradient evaluation

Gradients of the flow variables are particularly needed inside each control volume to formulate the linear reconstruction for second-order spatial accuracy of upwind schemes. Gradients of the velocity components and the temperature are also required for the evaluation of the viscous fluxes. TAU provides two approaches to evaluate gradients of flow variables. The first one is based on the Green-Gauss theorem and the second utilizes the least square method.

Using the Green-Gauss approach the gradient of a flow variable is approximated at each control volume center under taking into account the neighboring control volumes. Barth and Jespersen[9] formulated the approach such that it becomes compatible with the edge-based data structure requiring direct neighbor information only. Two control volumes are direct neighbors if they share a face of the computational mesh. For the cell-vertex discretization the Green-Gauss construction is exact only for linear functions only on triangular meshes. For the cell-centered discretization the construction is generally not exact for linear functions on quadrilaterals or triangles. Only if an edge of neighboring triangle cell centers is bisected in the computational grid, the construction becomes exact for linear functions on triangles [10].

The least-square approach seeks to find the gradient vector of a flow variable at each control volume center which minimizes the least square error with respect to the differences between neighboring variables and the variable itself [11]. The construction may include geometrical weights on the error terms. Hence one differentiates between unweighted and weighted least-square approaches. Weighted least-square gradients are normally used for meshes with highly stretched cells [10]. TAU uses an inverse distance weighting least-square approach in both the cell-vertex and the cell-centered grid metric.

The least-square construction represents a linear function exactly for the cell-vertex and cell-centered discretization on arbitrary mesh types. It is based on a stencil which identifies relevant neighboring points for use in the gradient evaluation. The stencil can be chosen arbitrarily. The choice of the stencil has strong influence on the robustness and accuracy of the numerical result. In TAU-CV and TAU-CC (Figure 4(a)) the stencil

of the considered control volume variable is formed by direct neighbors. This stencil is a satisfying choice for the cell-vertex grid metric. For the cell-centered grid metric a direct neighbor stencil can enforce decreasing robustness and decreasing accuracy. An example of such a stencil topology is shown in Figure 4(c) for a triangular mesh part. A stencil with only three neighbors is obtained. The least-square construction exhibits poor accuracy in this case, since there are no close points to provide accurate normal derivative information [10]. An alternate stencil includes all of the cells that share a vertex with the cell whose gradient is desired (Figure 4(b)), resulting in a robust but expensive method for computing the least-square gradient.

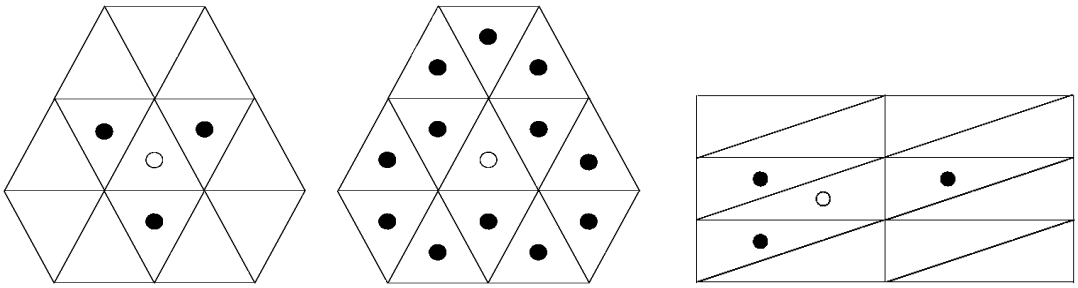

(a) Direct neighbors (b) Vertex neighbors (c) Non robust stencil

Figure 4: Stencil for least-square gradient calculation on cell-centered grid metric

A satisfying least-square stencil concerning efficiency, robustness and accuracy for TAU-CC is still under investigation. It should extend the direct neighbor stencil by vertex neighbors which increase accuracy and robustness. Diskin[2] suggested a promising approach. He uses smart augmentation that relates the stencil members to the discretization scheme of the convective terms.

2.4 Boundary treatment

When using the cell-vertex grid metric, the flow variables are stored directly on the boundary vertices, so the Dirichlet boundary conditions can be implemented on corresponding boundary points explicitly. On the contrary, the application of Newman boundary conditions can be realized more simply and reasonably in the cell-centered grid metric. Taking the numerical treatments of the no-slip wall boundary condition as an example, in TAU-CV, the residuals of the momentum equations should be set to zero in order to keep the non-slip condition. Further more, if we assume that the pressure gradient normal to the wall is zero and the wall temperature is known, the density and energy on the non-slip wall can also be specified directly. Thus the residuals at wall boundary points need not to be calculated any more. In TAU-CC, the fluxes over solid wall boundary faces have an important influence on the residuals of corresponding control volumes. To calculate these fluxes, the pressure and velocity gradients on the wall boundary should be evaluated with caution, which results in a complex boundary treatment.

At the intersection points or lines of faces with different boundary conditions (e.g. the diamond point in Figure 5), the above inherent advantage of the cell vertex method may cause conflict-defined boundary conditions. To avoid this problem, an approximate treatment should be used at intersection area of faces with boundary conditions. On the other hand, conflict-defined boundary conditions never occur in the cell-centered grid metric.

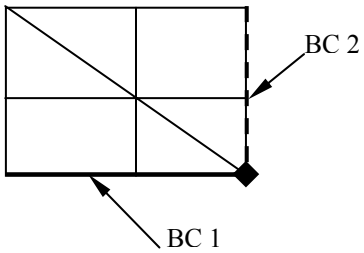

Figure 5: Illustration of the conflict-defined boundary condition in the cell-vertex grid metric

3 TEST CASES AND RESULTS

The TAU-Code covers a wide range of applications and offers various features and alternative approaches with respect to mesh handling, physical modeling and numerical schemes. The assessment of TAU-CC and TAU-CV has been restricted so far to some basic features. In this paper, the results obtained for selected representative test cases are shown.

3.1 Turbulent flat plate

Turbulent flow over a flat plate is an ideal case to test the basic performance of the flow solver. The computational region in this test case is a rectangle (see Figure 6), where the inlet is located two plate lengths L upstream of the leading edge and outlet is defined at the plate trailing edge. The height of the domain is 0.8L. Structured grid consisting 224×160 cells is used. The computations have been carried out for a Mach number of M_∞=0.30, and Re=5.0×10^6 based on the length of plate.

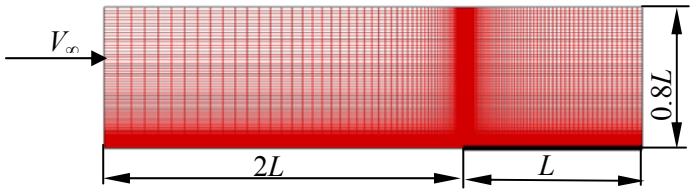

Figure 6: Mesh over turbulent flat plate

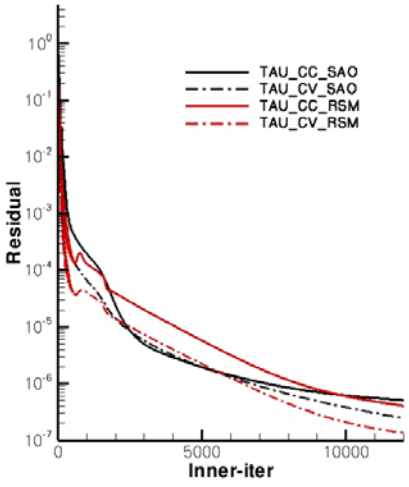

Figure 7: Convergence histories of turbulent flat plate test case

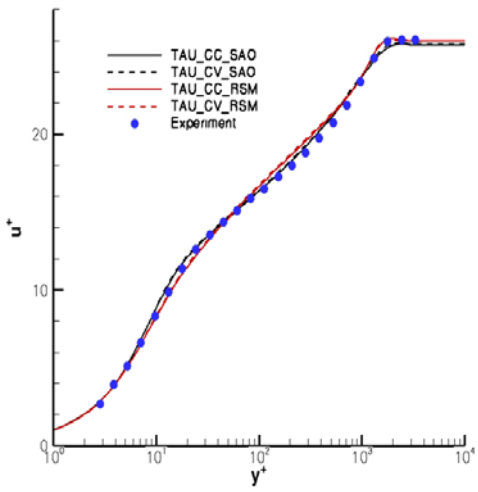

Figure 8: Comparison of velocity distribution at x/L=0.5

Figure 7 shows convergence histories for TAU-CC and TAU-CV with Spalart-Allmaras turbulence model (SAO) [8] and Reynolds stress turbulence model (RSM) of Wilcox [12]. As one can see, TAU-CV has faster convergence rate in this test case. Figure 8 shows the computed axial velocity distribution in the middle of the plate (at x/L=0.5) in comparison with experimental data [13]. These results are plotted as u^+ vs. y^+, where

$$u^+ = \frac{\widetilde{U}}{u_\tau} = \sqrt{\frac{2}{c_{f,\infty}}}\frac{\widetilde{U}}{U_\infty}\ , \quad \text{and} \quad y^+ = \sqrt{\frac{c_{f,\infty}}{2}}\,\mathrm{Re}_\infty\left(\frac{y}{L}\right)$$

For a given turbulence model TAU-CC and TAU-CV show nearly the same velocity profile. There are slightly differences between the different turbulence models. Clearly, the influence of grid metric on convergence solution could be ignored compare to the stronger impact of turbulence model. The conclusion drawing from this test case is that on a structured mesh with high quality, the discretization accuracies of TAU-CC and TAU-CV are almost identical, because the numbers of degrees of freedom involved in discretization are the same.

3.2 TC11 airfoil

The three element airfoil TC11 consists of a main airfoil with deflected slat and flap. For this test case, simulations were carried out at Mach number of M_∞=0.22, Reynolds number of Re=5.0×10^6 and attack angle of α=24.4°. The flow field around this airfoil is known to have very steep velocity gradients and strong interactions between different turbulent shear layers. The Wilcox k-w two-equation turbulence model [12] is used. A hybrid unstructured grid (see Figure 9), which consists of 18140 quadrangles in semi structured layers near the solid wall boundary and 32466 triangles in remaining computational domain, is used. Computations have been performed with both TAU-CC and TAU-CV. For the calculation of the convective flux, the central scheme [14] and the second order Roe upwind scheme [15] are used. The LU-SGS implicit scheme together with 3 levels V-cycle multigrid has been selected as time integration method and least-square method has been used for gradients evaluation in all computations.

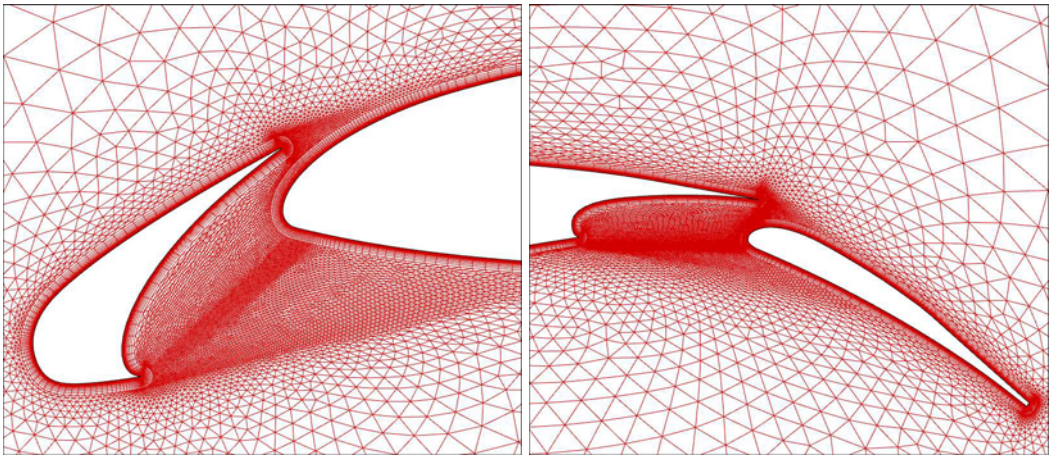

Figure 9: Hybrid unstructured mesh for TC11 airfoil

The comparison of the convergence histories is shown in Figure 10. The convergence behavior of TAU-CC and TAU-CV are comparable if they are measured by number of iterations. While considering the CPU time, TAU-CV is more efficient because less unknowns are involved in the computations. The comparison of the results of above

calculations and experimental data [16] is shown in Figure 11. As one can see, the pressure distributions show good agreements between numerical results and experimental data on slat and main element. However, less satisfactory agreement has been obtained on the upper side of the flap which maybe caused by the relatively coarse mesh on that area. Comparison of the computed aerodynamic coefficients and experimental data is shown in Table 1. As one can see, the results of TAU-CC with 2nd order upwind scheme shows better agreement with experiment.

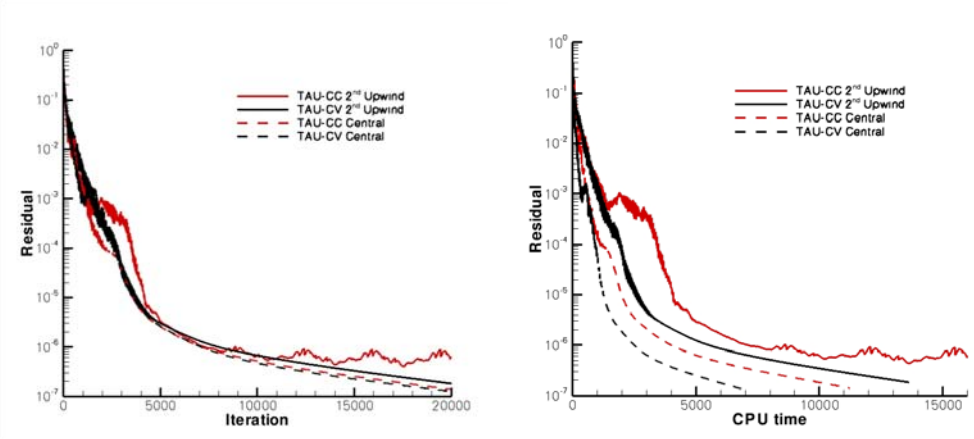

Figure 10: Convergence histories of TC11 airfoil computations

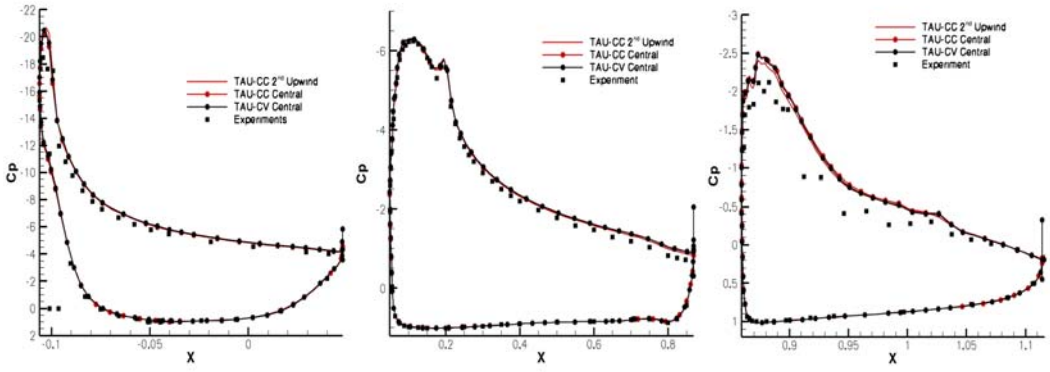

(a) On the slat (b) On the main element (c) On the flap

Figure 11: Comparison of computed surface pressure distributions between different computations on TC11 airfoil.

	TAU-CV central	TAU-CC central	TAU-CV 2nd upwind	TAU-CC 2nd upwind	Experiment
C_l	3.7020	3.6833	3.7744	3.6727	3.4944
C_d	0.1239	0.1337	0.1205	0.1112	0.1060

Table 1: Comparison of computed aerodynamic coefficients on TC11 airfoil

3.3 LANN wing

The LANN wing [17] has been used mostly as an unsteady flow test case. In this paper, a steady case of LANN wing at Mach number M_∞=0.82, Reynolds number Re=7.3×10^6 and attack angle of α=2.6° is selected to evaluate the performance of TAU-CC and TAU-CV. Two structure-type grids are used. The main difference between these two grids is the treatment of wing tip and trailing edge. Grid A, as shown in

Figure 12, simply sew up the wing upper and lower surface at tip and trailing edge, while grid B, keep the exact configuration at the wing tip and trailing edge by using multi-block grid. All simulations in this test case use Spalart-Allmaras one equation turbulence model, central scheme for convective flux calculation, LU-SGS as time stepping scheme and multigrid method to accelerate convergence. On grid A, bad convergence behavior was observed for TAU-CV, full multigrid must be used for it, and relatively smaller CFL number (approximately 5) should be used in order to achieve stability, while TAU-CC has no such limitation. The reason for this limitation has been pointed out in section 2.1. Therefore, the convergence speed of TAU-CV on grid A is slower than TAU-CC, as one can see in Figure 13(a). On grid B, both TAU-CC and TAU-CV have no convergence problems. As shown in Figure 13(b), the convergence of TAU-CV on grid B is a little faster than TAU-CC.

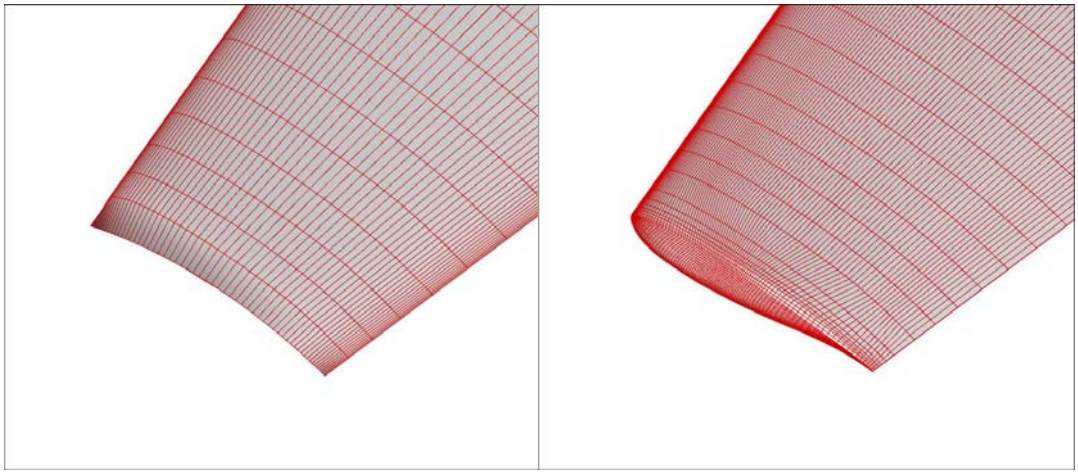

Grid A Grid B

Figure 12: Surface mesh at the tip of LANN wing

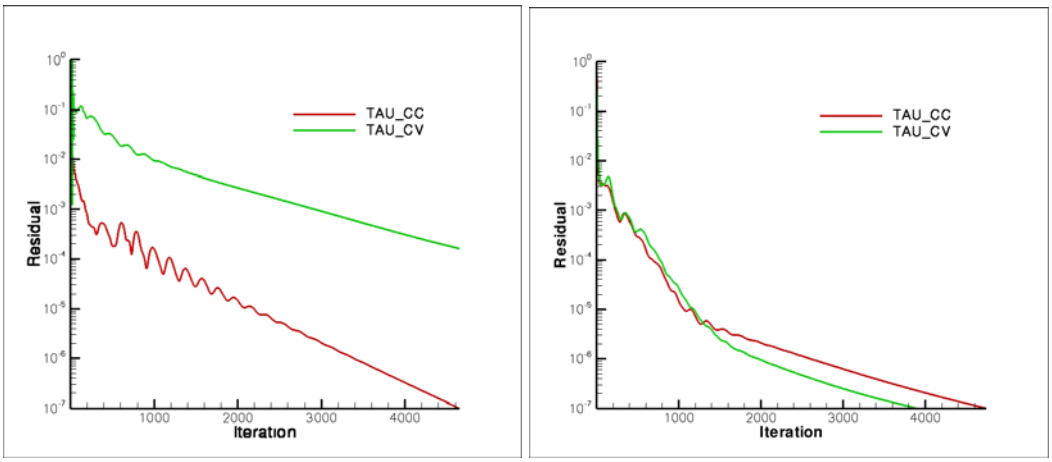

(a) On grid A (b) On grid B

Figure 13: Convergence histories for LANN wing test case.

Figure 14 shows the comparison of pressure distributions at 65% span obtained with TAU-CC and TAU-CV on the above two grids. In general, all computed results agree well with experiment data. Considering the details, TAU-CC predicts nearly the same shock position on both grids, whereas TAU-CV does not. In contrast, the pressure distributions predicted by TAU-CC have better agreement with experiment at lower

surface of LANN wing, while at the blunt trailing edge of grid B, result of TAU-CV seems to be more accurate.

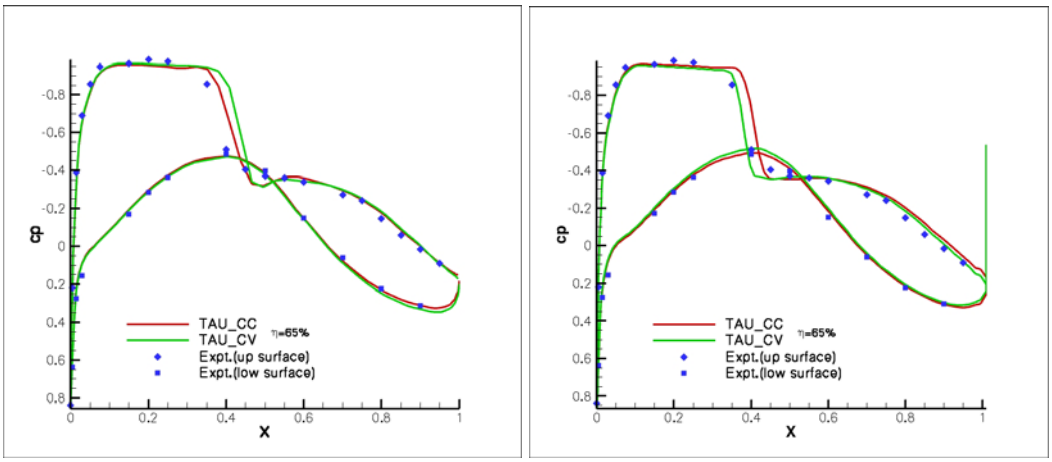

(a) On grid A (b) On grid B

Figure 14: Comparison of computed surface pressure distributions at 65% span-wise station.

3.4 DWP3-W1 wing

The DWP3-W1 wing, which was defined by the 3rd AIAA drag prediction workshop committee, is selected as a test case for investigating the grid convergence performance of TAU-CC and TAU-CV. A set of self-similar hybrid unstructured grids consists of three grid levels (coarse, medium and fine), has been generated by DLR in the drag workshop, directly used here. Basic information of these grids in cell-centered and cell-vertex grid metrics has been listed in Table 2, the surface mesh of medium grid is depicted in Figure 15.

	Coarse		Medium		Fine	
	TAU-CC	TAU-CV	TAU-CC	TAU-CV	TAU-CC	TAU-CV
Prisms	1976700		6784770		15052013	
Tetrahedrons	6710084		10672069		14931077	
Degrees of freedom	8686784	2174364	17456839	5288507	29983205	10150588
Number of faces	18279351	11932064	38154061	26289732	67199144	47832250
Number of wall faces	98835	49489	226159	113182	373291	186787

Table 2: Description of three levels of DWP3-W1 wing grid

The computations are conducted at Mach number M_∞=0.76, Reynolds number Re=5.0×10^6 and attack angle of α=0.5°. All simulations for this test case use the Menter SST two-equation turbulence model [18], 2nd order Roe scheme together with least-square gradient evaluation, LU-SGS time stepping and 3V-type multigrid method. In Figure 16, the pressure coefficients at 70% span computed by TAU-CC and TAU-CV on the coarse mesh are compared. The main differences can be found at the shock position and the trailing edge. The idealized parasite drag predicted by TAU-CC and TAU-CV versus grid index factor, defined as N$^{-2/3}$, have been shown in Figure 17. This figure suggests that more accurate parasite drag coefficients could be obtained on same grid using TAU-CC, mainly due to a larger number of unknowns involved in the computation.

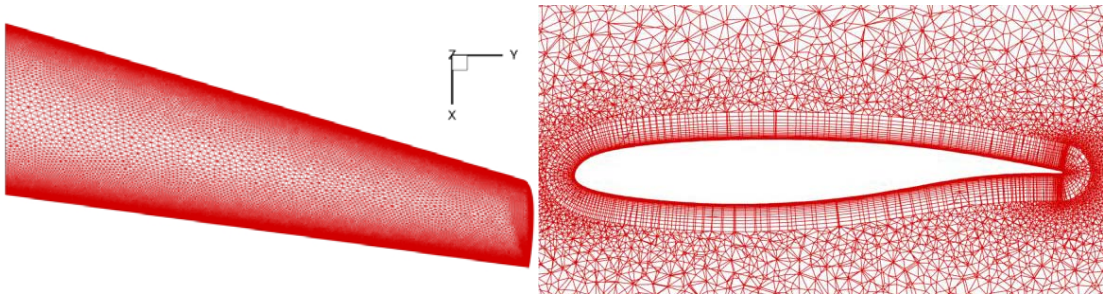

(a) Surface grid (b) Field slice at 70% span

Figure 15: Medium grid for DPW3-W1 wing.

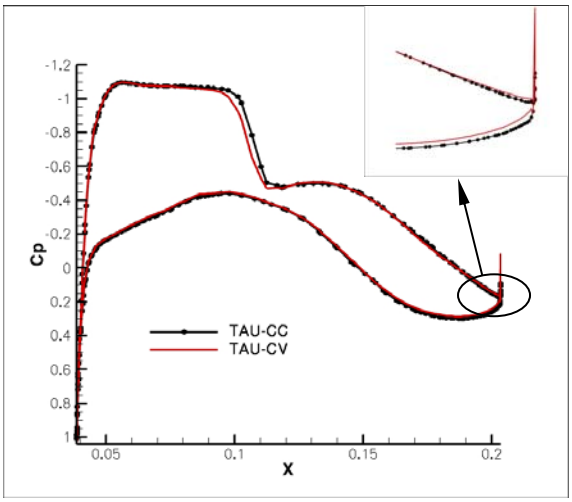

Figure 16: Comparison of computed pressure distribution at 70% span on coarse mesh.

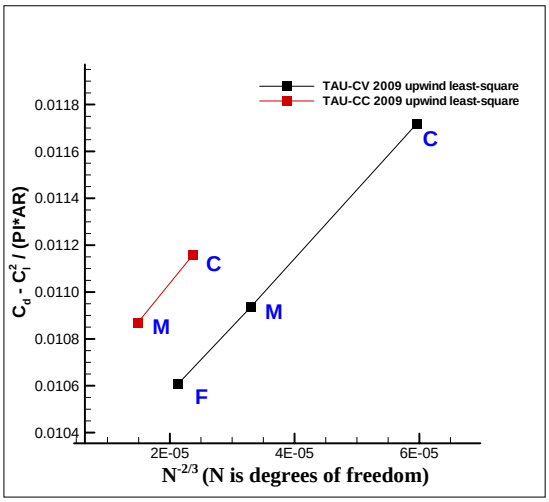

Figure 17: Comparison of grid convergence of parasite drag for TAU-CC and TAU-CV.

3.5 DLR-F6 wing-body with fairing

In this paper, the performance of the cell-centered and cell-vertex discretization on complex 3D configuration is evaluated by predicting the drag polar of the DLR-F6 FX2B wing-body configuration at Mach number M_∞=0.75, Reynolds number Re=5.0×10^6. The computational grid used here (as shown in Figure 18), is the coarse mesh generated by the Boeing Company in the 3rd AIAA drag prediction workshop [7]. It is worth noting that this mesh has a large number of highly stretched cells at the leading edge region, which is very suitable to demonstrate the robustness of the TAU-Code. All calculations in this test case were conducted with the upwind scheme together with least-square gradients, and the Spalart-Allmaras turbulence model. Figure 19 shows the predicted drag polar of TAU-CC and TAU-CV compared to the wind tunnel measurements [19]. Since the coarse mesh was used here, there are slight differences between the numerical results and experimental data, while the result of TAU-CC shows a somewhat better agreement with experiment.

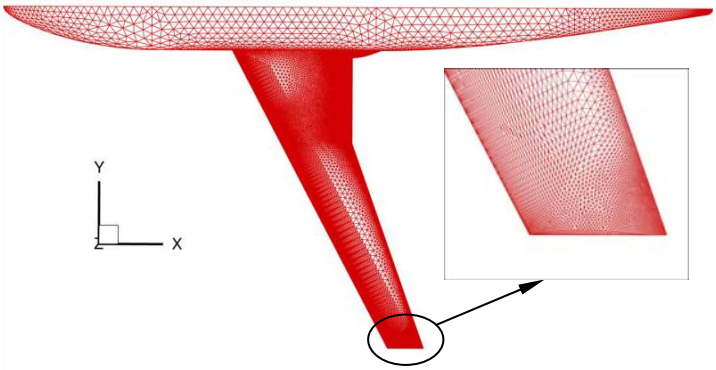

Figure 18: Surface mesh of DLR-F6 with FX2B fairing generated by Boeing Company

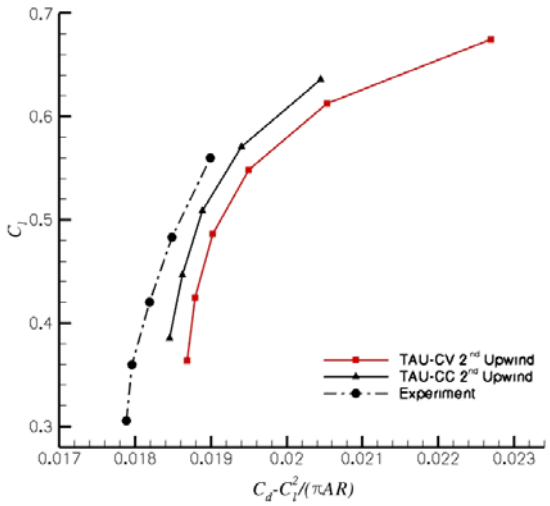

Figure 19: Comparison of idealized parasite drag coefficient versus lift coefficient between computations and experiment for DLR-F6 with FX2B fairing.

4 CONCLUSIONS

Based on the DLR TAU-Code, a comparison and evaluation of the cell-centered and cell-vertex discretization were conducted by using a series of test cases. The results indicate that the cell-centered scheme (TAU-CC) and the cell-vertex scheme (TAU-CV) have nearly the same accuracy and efficiency for most of the structured grid test cases. This is expected since the number of degrees of freedom are the same. For the test cases with unstructured grid, second-order upwind scheme with least square gradient reconstruction is strongly suggested to be used in TAU-CC, in order to achieve accurate results. With this premise, in general TAU-CC is less efficient but more acurate compared to TAU-CV on the same mesh. It is also observed that TAU-CC has better performance for configuration with sharp tailing edge or wing tip, while TAU-CV is more suitable for dealing with blunt tailing edge configuration.

The general conclusion is that TAU-CC has strong capability for the simulation of turbulent flows and this additional option provides the TAU-Code extended powerful functionalities for the simulation of complex flow problems.

REFERENCES

[1] D. J. Mavriplis, Unstructured-Mesh Discretizations and Solvers for Computational Aerodynamics, AIAA Journal, vol. 46 no. 6, pp.1281–1298 (2008)

[2] B. Diskin, Comparison of Cell-Centered and Node-Centered Unstructured Finite-Volume Discretizations: Inviscid Fluxes, AIAA paper 2010-1079, 2010.

[3] B. Diskin, J. Thomas, E. Nielsen, J. White and H. Nishikawa, Comparison of Node-Centered and Cell-Centered Unstructured Finite-Volume Discretizations Part I: Viscous Fluxes, AIAA paper 2009-597, 2009.

[4] R. C. Swanson and R. Radespiel, Cell Centered and Cell Vertex Multigrid Schemes for the Navier-Stokes Equations, AIAA Journal, vol. 29 no.5, pp.697–702 (1991)

[5] D. Schwamborn, T. Gerhold and R. Heinrich: *The DLR TAU-Code: Recent Applications in Research and Industry*. In proceedings of "European Conference on Computational Fluid Dynamics" ECCOMAS CDF 2006, Delft The Netherland, 2006

[6] T. Gerhold, M. Galle, O. Friedrich and J. Evans, Calculation of Complex 3D Configurations Employing the DLR TAU-Code, AIAA paper 97-0167, 1997.

[7] "3rd AIAA CFD Drag Prediction Workshop." San Francisco, 2006, http://aaac.larc.nasa.gov/tsab/cfdlarc/aiaa-dpw/Workshop3.

[8] P.R. Spalart, and S.R. Allmaras, A One-Equation Turbulence Model for Aerodynamic Flows, Recherche Aerospatiale, **1**, pp. 5-21 (1994)

[9] T.J. Barth, and D.C. Jespersen, The Design and Application of Upwind Schemes on Unstructured Meshes, AIAA Paper 89-0366, (1989)

[10] D. J. Mavriplis, Revisiting the Least-square Procedure for Gradient Reconstruction on Unstructured Meshes, NASA/CR-2003-212683, NIA Report No. 2003-06, (2003)

[11] T. J. Barth, A 3-D Upwind Euler Solver for Unstructured Meshes, AIAA Paper 91-1548. (1991)

[12] D.C. Wilcox, Turbulence Modeling for CFD, 2nd Edition, DCW Industries, Inc., La Canada CA. (1998)

[13] K. Wieghardt and W. Tillman, On the Turbulent Friction Layer for Rising Pressure, NACA TM-1314 (1951)

[14] A. Jameson, W. Schmidt, and E. Turkel, Numerical Solution of the Euler Equations by Finite Volume Methods Using Runge-Kutta Time Stepping Schemes, AIAA Paper 81-1259. (1981)

[15] P.L. Roe, Characteristic Based Schemes for the Euler Equations, Annual Review of Fluid Mechanics, **18**, pp. 337-365. (1986)

[16] L. Cambier and N. Kroll, MIRACLE-a joint DLR/ONERA effort on harmonization and development of industrial and research aerodynamic computational environment, Aerospace Science and Technology, Volume 12, Issue 7, pp. 555-566 (2008)

[17] I.R.J. Zwaan, LANN Wing Pitching Oscillations, Compendium of Unsteady Aerodynamic Measurements, AGARD-R-702. (1982)

[18] F. R. Menter, Two-Equation Eddy-Viscosity Turbulence Models for Engineering Applications, AIAA Journal, Vol. 32, No. 8, pp. 1598-1605. (1994)

[19] G. M. Gatlin, M. B. Rivers, S. L. Goodliff, R. Rudnik and M. Sitzmann, Experimental Investigation of the DLR-F6 Transport Configuration in the National Transonic Facility, AIAA Paper 2008-6917. (2008)